Electronic structure and optical properties of As-rich reconstruction phases of $Ga_{0.5}Al_{0.5}As$ (100): A first-principles research

XIAOHUA YU[a,*], ZUDE JIN[a], FANG LIU[b], GUIRONG SHAO[a], HUIXIA SUN[a]
aDepartment of Physics and Electronic Engineering, Yuncheng University, Yuncheng 044000,China
bCollege of Artificial Intelligence, Wuhan Technology and Business University, Wuhan 430065, China

Four As-rich reconstruction models: α(2×4), β1(2×4), β2(2×4) and γ(2×4) phases are built, using first-principles method, electrical structure and optical properties of these four phases are researched. Results show that β2(2×4) is the most easily formed reconstructed phase. Sp3 hybrid orbital is changed when the reconstructed phases are formed. The electron transition from VBM to CBM of α(2×4) is the easiest while the photoemission of γ(2×4) phase is easiest. During the formtion of the phases, the metal reflection characteristic region moves towards the lower energy end and the energy range of the metal reflection characteristic region becomes smaller. β2 (2×4) phase is the most favorable to the transmission of photons.

1. Introduction

In 1963, S.Q. Duntely found that in the sea water the decay of light with wavelength of 470~580 nm was the weakest [1], as a result, the blue-green light sensitive underwater photodetector is of great significance in ocean exploration, ocean communication and seabed imaging. In the underwater photoelectric detection equipment, 532 nm laser is mainly used as the light source, and the photocathodes used mainly include Na_2KSB-Cs, GaAs, GaAsP and GaAlAs. Among these photocathodes, GaAlAs is the most suitable since that only GaAlAs can be used to prepare narrow-band photocathode, which only sensitive to light arround 532 nm. In 1974, Martinelli et al. prepared reflective NEA $Ga_{1-x}Al_xAs$ (x=0.3) photocathode for the first time [2]. In 2009, Nishitani et al. prepared a reflective GaAlAs photocathode using $Ga_{1-x}Al_xAs$ (x = 0.28) bulk material [3]. In 2013, Chen et al. prepared a narrow band $Ga_{0.37}Al_{0.63}As$ photocathode with a wavelength range of 450~600 nm [4].

GaAlAs photocathode is prepared on As-rich GaAlAs(100) surface, according to the "Electron Countong Rule" [5], surface relaxation [6], surface reconstruction [7,8], usually exist at the surface. At present few research has been conducted on As-rich GaAlAs(100) surface. GaAlAs and GaAs have the same lattice structure, so we can learn from the research results of the surface structure of As-rich GaAs (100). The reconstructed phases of as-rich GaAs (001) surface mainly include C (4×4) at 7/4mL (monolayers), γ (2×4) at 1mL, β1 (2×4) at ¾mL, β2 (2×4) at ½mL and α (2×4) at ½mL. Among them, (2×4) reconstruction exists in a large surface coverage area of As, which is the most common reconstruction structure. In this manuscript, models of As-rich GaAlAs(100) α(2×4), β1(2×4), β2(2×4) and γ(2×4) reconstruction phases are built, first-principles method is used to analyze the electrical structure and optical properties [9]. Based on the calculation results, the reconstructed phase with the best photoemission performance is determined, providing theoretical guidance for the preparation of GaAlAs (100) photocathodes.

2. Calculated method and models

In our calculation, the ratio of Al is taken as 0.5, labeled as $Ga_{0.5}Al_{0.5}As$. Since the influence of Al and Ga atoms location distribution on the calculation result is negligible [10], in this manuscript Al and Ga atoms are uniformly distributed. As shown in Fig. 1, slab model is used and each reconstruction models contain 7 atom layers (4 As atom layers and 3 Ga/Al atom layers). A(2×4) phase contains 28 As atoms, 12 Ga atoms and 12 Al atoms. B1(2×4) phase contains 30 As atoms, 12 Ga atoms and 12 Al atoms. B2(2×4) phase contains 28 As atoms, 11 Ga atoms and 11 Al atoms. Γ(2×4) phase contains 32 As atoms, 12 Ga atoms and 12 Al atoms. The dangling bonds at the bottom are saturated with a layer of fractionally charged (Z=0.75) [11] hydrogen like pseudoatoms.
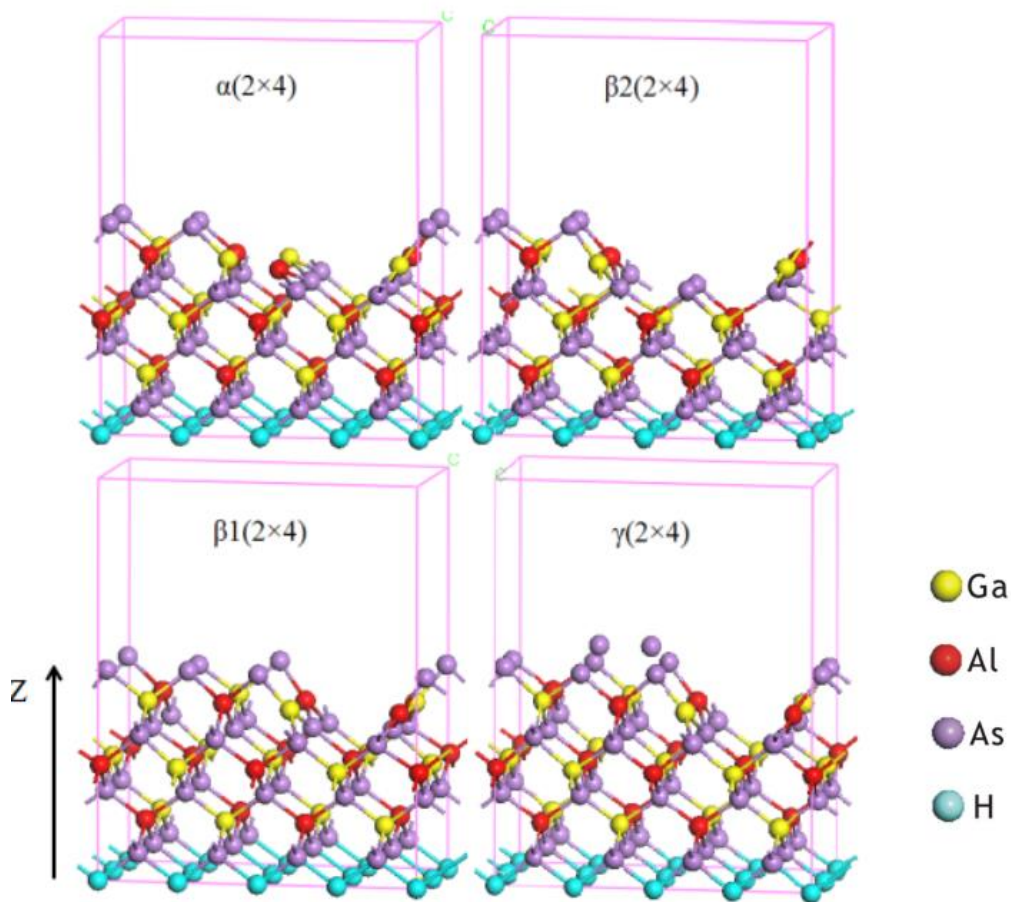
Fig. 1. Models of $Ga_{0.5}Al_{0.5}As(100)$ $\alpha(2\times4)$, $\beta1(2\times4)$, $\beta2(2\times4)$ and $\gamma(2\times4)$ phases (color online)

Our calculations are carried out by density functional theory (DFT) within the generalized gradient approximation (GGA) [12,13], which is implemented in the CASTEP codes [10,14]. In our calculation, the lower three atom layers are fixed to simulate the bulk circumstance, the upper four layers are allowed to relax freely. A vacuum layer with width of 10 nm is added along z axis. The interaction between the core and valence electrons is described by the ultra-soft pseudopotential generating from Ga:$3d^{10}4s^24p^1$, Al:$3s^23p^1$, As:$4s^24p^3$ and H:$1s^1$. During the iteration process, the convergence precision is set as 2×10^{-6} eV/atom, the convergence criteria of interatomic forces is set as 0.005 eV/nm, the convergence criteria of stress is 0.05 Gpa, the convergence criteria of single atom energy is 1.0×10^{-5} eV/atom, the convergence criteria of maximum atom displacement is 0.0001 nm, k grid is set as $6\times4\times1$, plane wave cut-off energy is set as 330 eV, all the calculation is performed in the reciprocal space [15,16], scissors operator correction is used in the calculation of optical properties.

In addition, to research the change of electronic structure and optical properties during the formation of the surface, a bulk model of 32 As atoms, 16 Al atoms and 16 Ga atoms with Al and Ga atoms are uniformly distributed

is built, in bulk model calculation, k grid is set as $5\times5\times5$, the other parameters are the same as the slab model calculation.

3. Results and discussion

The cohesive energy of per atom can be used to analyze the stability of one model. It can be calculated by the following formula:

$$E_{coh} = \frac{E_{slab}^{total} - \sum_i N_i E_i}{\sum_i N_i} \quad (1)$$

where, E_{slab}^{total} is the total energy of the slab model, E_i represents the energy of atom I and N_i represents the number of atom i. The calculated cohesive energy of $\alpha(2\times4)$, $\beta1(2\times4)$, $\beta2(2\times4)$ and $\gamma(2\times4)$ phases are shown in

Table 1. Minus value means that the model is stable, the smaller the minus value, the more stable the model is. Results show that α(2×4), β1(2×4), β2(2×4) and γ(2×4) phases are all stable and β2(2×4) phase is the most stable one, showing that β2(2×4) is the most easily formed reconstructed phase.

Table 1. Cohesive energy (in unit of eV/atom) and work function (in unit of eV) of α(2×4), β1(2×4), β2(2×4) and γ(2×4) phases

phases	α(2×4)	β1(2×4)	β2(2×4)	γ(2×4)
E_{coh}	-4.605	-4.651	-4.673	-4.657
Φ	4.896	4.961	4.797	4.708

3.1. Density of states

Density of states (DOS) can be used to analyze the electron distribution of the phases, Fig. 2 depicts the DOS curves of four phases, both total density of states (TDOS) and partial density of states (PDOS) of each atom are collected. TDOS curves show that the valence band of four phases are consist of the lower valence band (located at -15.8~-8.8eV) and upper valence band (located at -6.9~0eV). There are sharp DOS peaks at about -14.5eV for all the phases, -14.5eV peak locations and peak values of four phases are different. The valence band maximum (VBM) is mainly formed by As 4p state and Al 3p state, conduction band minimum (CBM) is mainly formed by Al 3P state.

The surface morphology of different reconstructed phases resulted in the difference of DOS curves. In order of α (2×4), β1 (2×4), β2 (2×4) and γ (2×4), the peaks value of Ga 3d state near -14.5eV decreased in turn, and the half-peak width increased in turn. Ga 3d peak of γ (2×4) phase splits into two peaks. In the range of -12.3~-8.5eV, the density of As 4s states of each phase are obviously different. The double peak of α (2×4) phase is the most gentle, and γ (2×4) phase appears two more peak than other phases. The Al 3s peak of β2 (2×4) phase in the energy range of -6.6~-3.7eV is significantly higher than that of other phases, and α (2×4) phase in the energy range of -6.6~-3.7eV has one more peaks than other phases. In the energy range of -3.8~0eV, As 4p peak of γ (2×4) phase splits into many small peaks.
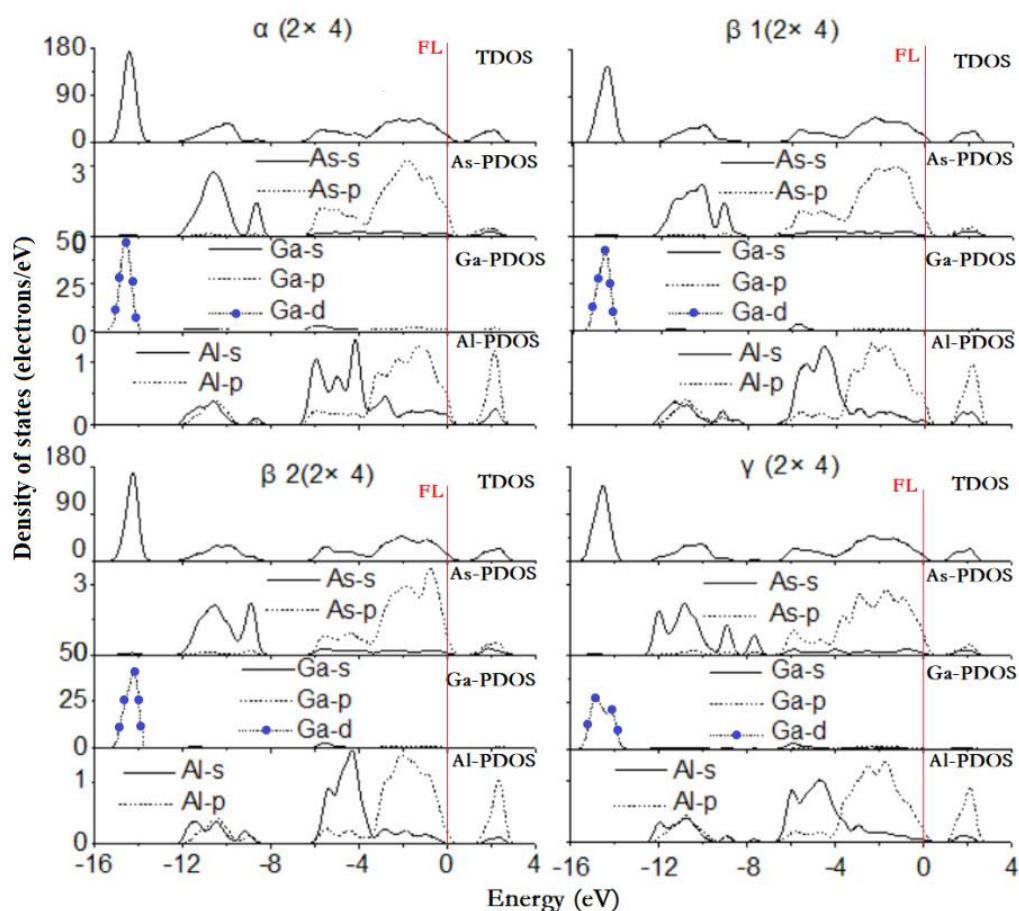

Fig. 2. DOS curves of Ga$_{0.5}$Al$_{0.5}$As(100) α(2×4), β1(2×4), β2(2×4) and γ(2×4) phases (color online)

The percentage of electron change in each state was obtained by integrating the density curve of states and are compared with the bulk material, as shown in Table 2. To maintain the stability of the surface, electron transfer occurs at the surface to eliminating the dipole moment, resulting in the change of electron distribution of four phases. The electrons at the surfaces is reduced compared to the bulk, in the order of β1(2×4), α(2×4), β2(2×4) and γ(2×4), the decrement increases in turn. It can be seen from the table that in the phases, s and p state of Ga, Al and As atoms are all smaller than the bulk, Ga 3d state electrons in four phases is almost the same as in the bulk.

The calculated results show that the sp3 hybrid orbital is changed when the reconstructed phases are formed, the cubic sp3 hybrid orbital of Al atoms have the tendency of turning to the plane sp2 hybrid orbital, the change in α(2×4) phase is the most obviously.

Table 2. Electronic changes of α(2×4), β1(2×4), β2(2×4) and γ(2×4) phases compared to the bulk

phases		α(2×4)	β1(2×4)	β2(2×4)	γ(2×4)
TDOS		-11.71%	-9.05%	-13.26%	-18.02%
As	s	-7.11%	-6.30%	-2.98%	-1.25%
	p	-4.38%	-4.99%	-6.49%	-9.15%
Ga	s	-8.60%	-8.85%	-8.93%	-11.28%
	p	-5.20%	-4.48%	-4.34%	-7.06%
	d	+0.17%	+0.16%	+0.23%	-0.05%
Al	s	-5.72%	-5.88%	-7.19%	-10.34%
	p	-10.13%	-10.11%	-9.48%	-11.28%

3.2. Band structure and work function

In Fig. 2 red lines show the Fermi level, the Fermi level is located at 0eV, and the VBM of the bulk is also located at 0eV. From Fig. 2 we can see that the VBM of the four reconstructed phases all move towards the higher energy level, and the Fermi energy levels of four phases enter the valence band, forming the band bending region (BBR). The electrons at the surface is more easily to absorb photons and generate photoelectrons than electrons in the bulk. The difference between CBM and VBM of α(2×4) phase is the minimum, the electron transition from VBM to CBM of α(2×4) is the easiest.

After transition, the photoelectron still need to move to the surface and overcome the surface barrier before they can escape to form a photocurrent. For semiconductors, the work function is defined as the minimum energy needed by an electron at the bottom of the valence band to escape externally, and can be expressed as following formula [17]:

$$\Phi = E_{vac} - E_F \tag{2}$$

where, E_{vac} is the vacuum level, and E_F is the Fermi level. The calculated work function of α(2×4), β1(2×4), β2(2×4) and γ(2×4) phases are shown in Table 1. The lower the work function, the easier it is for photoelectrons to escape. Results shows that the work function of four phases are rather similar, the work function of γ(2×4) is the lowest, showing that the photoemission of γ(2×4) phase is easiest. The band structure is depicted in the Fig. 3, including the BBR, Fermi level, CBM, VBM and work function.

3.3. Optical properties

According to the definitions of direct transition probabilities and Kramers-Kronig dispersion relations, absorption coefficient, reflectivity can be calculated as following formulas [18,19]:
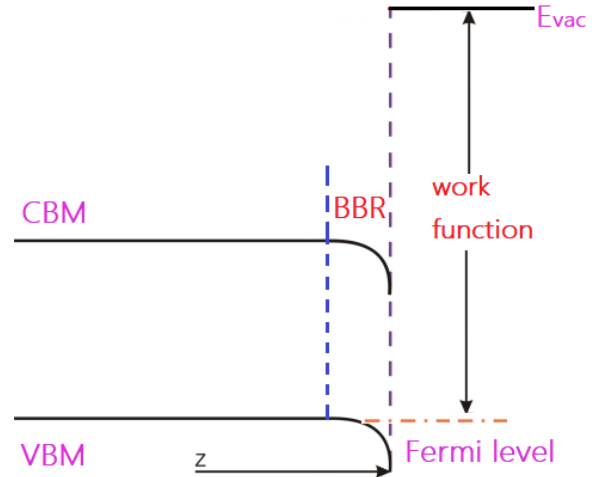

Fig. 3. Band structure at the surface (color online)

$$\alpha \equiv 2\omega k / c = 4\pi k / \lambda_0 \tag{3}$$

$$R(\omega) = [(n-1)^2 + k^2]/[(n+1)^2 + k^2] \tag{4}$$

where n is the refractive index, k is the extinction coefficient, λ_0 is the wavelength of light in vacuum.

The calculated dielectric functions of different phases are shown in Fig. 4. Compared with the bulk model, the surface dielectric function curve moves towards the low-energy end. The difference of dielectric function among four phases are mainly in low energy region of 0~6.1 eV. In the minus dielectric function region, the reflectivity is more than 80%, and the region is called metal reflection characteristic region. The metal reflection characteristic region of the bulk is 4.1~9.6 eV, and the metal reflection characteristic region of the reconstructed phases is 2.8~6.1 eV. Compared to the bulk, at the surface the metal reflection characteristic region moves towards the lower energy end, and the energy range of the metal reflection characteristic region becomes smaller.
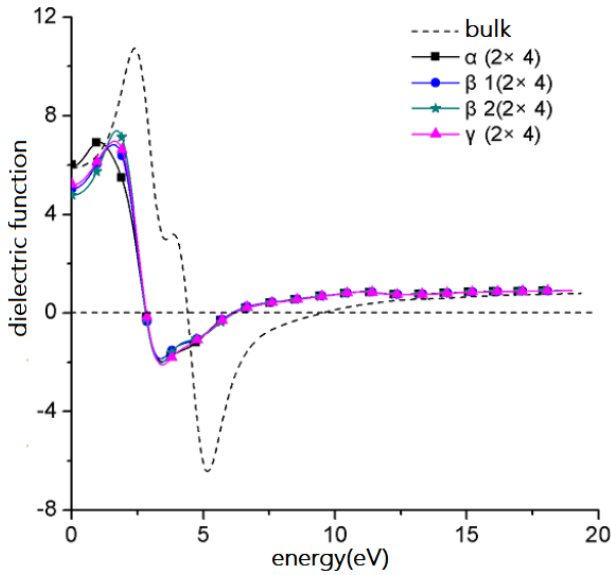

Fig. 4. Dielectric functions of α(2×4), β1(2×4), β2(2×4) and γ(2×4) phases (color online)

The calculated absorption coefficients and reflectivity curves of different reconstructed phases are shown in Fig. 5. The absorption peaks of the reconstructed phases move to the lower energy end, the absorption peaks location of α(2×4), β1(2×4), β2(2×4) and γ(2×4) phases are almost the same. The falling edges of reflectivity in the reconstructed phases move to lower energy side.

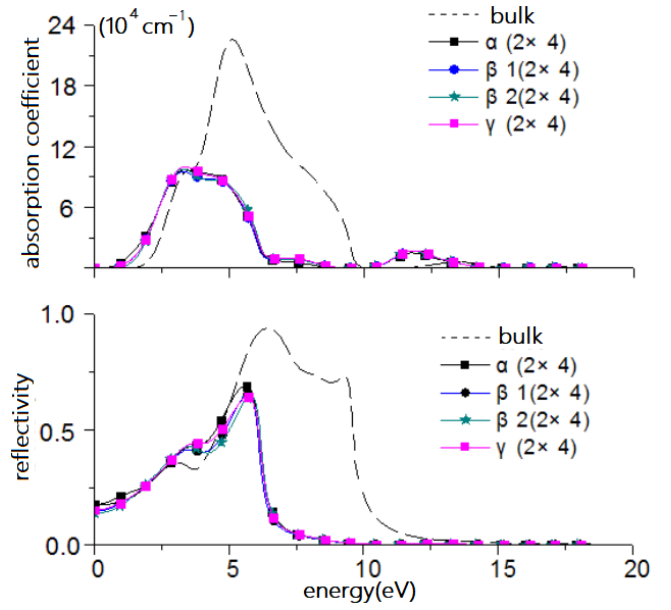*Fig. 5. Absorption coefficient and reflectivity of α(2×4), β1(2×4), β2(2×4) and γ(2×4) phases (color online)*

The percentage change of the average absorption coefficient and average reflectivity of the reconstructed phases compared to the bulk can be used to analyze the photon transmittance at the surface, the formulas are shown below:

$$\Delta A = \frac{\int a_{recon}(E)dE - \int a_{bulk}(E)dE}{\int a_{bulk}(E)dE} \qquad (5)$$

$$\Delta R = \frac{\int r_{recon}(E)dE - \int r_{bulk}(E)dE}{\int r_{bulk}(E)dE} \qquad (6)$$

where, a_{recon} represents the absorption coefficient at the surface. a_{bulk} represents the absorption coefficient of the bulk. r_{recon} represents the reflectivity at the surface. r_{bulk} represents the absorption coefficient of the bulk. The calculated results are shown in Table 3. The absorption coefficient and reflectivity at the surface are smaller than that in the bulk, which is favorable for photons to excite photoelectrons through the surface. The β2 (2×4) phase is the most favorable for the transmission of photons.

Table 3. The change of the average absorption coefficient and average reflectivity of four phases

phases	$\alpha(2\times4)$	$\beta1(2\times4)$	$\beta2(2\times4)$	$\gamma(2\times4)$
ΔA	-55.8%	-56.5%	-57.3%	-55.6%
ΔR	-51.8%	-55.5%	-55.0%	-53.7%

4. Conclusion

In this manuscript, first-principles method is used to analyze the electrical structure and optical properties of $Ga_{0.5}Al_{0.5}As$ $\alpha(2\times4)$, $\beta1(2\times4)$, $\beta2(2\times4)$ and $\gamma(2\times4)$ phases. Results show that $\alpha(2\times4)$, $\beta1(2\times4)$, $\beta2(2\times4)$ and $\gamma(2\times4)$ phases are all stable and $\beta2(2\times4)$ phase is the most stable, $\beta2(2\times4)$ is the most easily formed reconstructed phase. The calculated results show that the sp3 hybrid orbital is changed when the reconstructed phases are formed, the cubic sp3 hybrid orbital of Al atoms have the tendency of turning to the plane sp2 hybrid orbital, the change of $\alpha(2\times4)$ phase is the most obviously. The electron transition from VBM to CBM of $\alpha(2\times4)$ is the easiest while the photoemission of $\gamma(2\times4)$ phase is easiest. During the formation of the phases, the metal reflection characteristic region moves towards the lower energy end and the energy range of the metal reflection characteristic region becomes smaller. B2 (2×4) phase is the most favorable to the transmission of photons.

Acknowledgement

References

[1] S. Q. Duntley, Journal of the Optical Society of America **53**, 214 (1963).
[2] R. U. Martinelli, M. Ettenberg, J. Appl. Phys. **45**, 3896 (1974).
[3] T. Nishitani, M. Tabuchi, Y. Takeda, Y. Suzuki, K. Motoki, T. Meguro, Jpn. J. Appl. Phys. **148**, 06FF02 (2009).
[4] X. Chen, Y. Zhang, B. Chang, P. Gao, J. Zhao, F. Shi, Optoelectron. Adv. Mat. **6**(1-2), 307 (2012).
[5] G. P. Srivastava, Appl. Surrf. Sci. **252**, 7600 (2006).
[6] H. G. Ye, G. D. Chen, Y. L. Wu, Phys. Rev. B **78**, 193308 (2008).
[7] C. S. Davis, S. V. Novikov, T. S. Cheng, Journal of Crystal Growth **226**, 203 (2001).
[8] M. L. Wise, L. A. Okada, O. Sneh, J. Vacuum. Tech. **13**, 1853 (1995).
[9] Y. Ding, Y. Wang, J. Ni, L. Shi, S. Shi, W. Tang, Physica B: Condensed Matter. **406**, 2254 (2014).
[10] X. Yu, G. Shao, H. Sun, Optoelectron. Adv. Mat. **14**(3-4), 123 (2020).
[11] S. Krukowski, P. Kempisty, P. Strak, J. Appl. Phys. **105**, 113701 (2009).
[12] M. G. Brik, C. G. Ma, V. Krasnenko, Surf. Sci. **608**, 146 (2013).
[13] J. Perdew, K. Burke, M Ernzerhof, Phys. Rev. Lett. **77**, 3865 (1996).
[14] E. B. Kandemir, B. Gönül, G. T. Barkema, K. M. Yu, W. Walukiewicz, L. W. Wang, Comput. Mater. Sci. **82**, 100 (2014).
[15] C. Hogan, D. Paget, Y. Garreau, M. Sauvage, G. Onida, L. Reining, P. Chiaradia, V. Corradini, Phys. Rev. B **68**, 205313 (2003).
[16] G. Kresse, J. Hafner, Phys. Rev. B **47**, 558(R) (1993).
[17] A. L. Rosa, J. Neugebauer, Phys. Rev. B **73**, 205346 (2006).
[18] Q. Chen, Q. Xie, W. J. Yan, Sci. China (Ser. G) **38**, 825 (2008).
[19] Y. J. Du, B. K. Chang, H. G. Wang, J. J. Zhang, M. S. Wang, Opt. Lett. **10**, 051601 (2012).

---

*Corresponding author: 624554818@qq.com